

Applications of mesoporous silica encapsulated gold nanorods loaded doxorubicin in chemo-photothermal therapy

Nghiem Thi Ha Lien,¹ Anh D. Phan,^{2,3} Bui Thi Van Khanh,⁴ Nguyen Thi Thuy,¹ Nguyen Trong Nghia,¹ Hoang Thi My Nhung,⁴ Tran Hong Nhung,¹ Do Quang Hoa,¹ Vu Duong,¹ and Nguyen Minh Hue¹

¹*Center for Quantum and Electronics, Institute of Physics, VAST, Dao Tan 10, Hanoi 10000, Vietnam**

²*Faculty of Materials Science and Engineering, Phenikaa Institute for Advanced Study, Phenikaa University, Hanoi 12116, Vietnam[†]*

³*Faculty of Information Technology, Artificial Intelligence Laboratory, Phenikaa University, Hanoi 12116, Vietnam*

⁴*College of Science, Vietnam National University (VNU), Hanoi, 334 Nguyen Trai Road, Thanh Xuan, Hanoi, Vietnam*

(Dated: July 24, 2020)

We investigate chemo-photothermal effects of gold nanorods (GNRs) coated using mesoporous silica (mSiO₂) loading doxorubicin (DOX). When the mesoporous silica layer is embedded by doxorubicin drugs, a significant change in absorption spectra enable to quantify the drug loading. We carry out photothermal experiments on saline and livers of mice having GNRs@mSiO₂ and GNRs@mSiO₂-DOX. We also inject the gold nanostructures into many tumor-implanted mice and use laser illumination on some of them. By measuring weight and size of tumors, the distinct efficiency of photothermal therapy and chemotherapy on treatment is determined. We experimentally confirm the accumulation of gold nanostructures in liver.

I. INTRODUCTION

Photothermal effects of gold nanorods have been extensively investigated due to medical applications [1–6]. When shined by light, gold nanorods (GNR) absorb radiation and confine electromagnetic energy to the surface of a gold-dielectric interface. The absorbed energy is efficiently transformed into thermal energy and locally heats to a few hundred degree Celsiuses under illumination of laser light. Since destruction of living cells occurs at temperatures above 43 °C, this light-to-heat conversion process is used for cancer therapy [1–6]. In synthesis of gold nanostructures using cetyl trimethylammonium bromide (CTAB), their gold surfaces become unstable and easily aggregate. This aggregation causes the loss of unique optical properties. Moreover, it has been proved that CTAB is a highly toxic cationic surfactant [7, 8]. To exploit GNRs for biomedical applications, it is necessary to replace CTAB and coat GNRs by safer and more biocompatible materials/molecules. Recently, extensive efforts have been devoted to encapsulate GNRs with mesoporous silica [9, 10], bio-polymers [11, 12], or other composites [13, 14]. These coating materials can be easily combined with drugs or target molecules to functionalize GNRs.

In some biological and photothermal applications, GNRs is preferred rather than gold nanoshells (GNSs) because of two main reasons. First, the size of GNSs having plasmon resonances in the near-infrared region is large (~ 150nm) [15, 16], while the size of GNRs is small (≤ 80 nm) [1–6]. According to previous works [17, 18],

sub-100 nm nanoparticles are selected for treatments due to their free movement through tissues. Second, it is well known that GNRs have a strong optical absorption cross section and a very small scattering cross section [19, 20]. These behaviors are relatively opposite to properties of large size GNSs. Thus, the GNRs are more photothermally efficient than the GNSs [19, 20].

While doxorubicin is an anthracycline antibiotic known as one of the most therapeutic anti-tumor drugs to treat various solid malignant tumors. Doxorubicin intercalates within DNA helix in the cell nucleus. Thereby, this drug inhibits macromolecular biosynthesis and destroys DNA function [21]. However, free DOX has its own several side effects when used in cancer chemotherapy [22]. To reduce the toxicity and side effects and improve treatment efficiency, one encapsulates DOX in liposomes [23], loads onto silica mesoporous nanoparticles [24], or incorporates into nanocomposites such as silica mesoporous encapsulated GNRs [25], GNR@mSiO₂ or GNR@polymers [9, 12]. Doxorubicin release and loading from GNR@mSiO₂-DOX or GNR@polymer-DOX strongly depend on acidic medium and laser irradiation at surface plasmon resonances [9]. The synergistic effect of the drug loaded GNR@SiO₂ has been demonstrated [9, 14, 22].

There have recently been clinical trials for gold-nanoparticle-based photothermal cancer therapy to ablate thermally neck, brain, lung, and prostate cancerous tumors [9, 26–28]. These results showed promising scenarios since tumors were locally heated. However, accumulation of gold nanostructures in liver and spleen throughout life in bodies without excrete is the most weakest point of this approach [27, 28]. The penetration of gold composites into tumors is tiny compared to the infused initial counterparts.

In this work, we synthesize GNRs@mSiO₂-DOX and investigate photothermal and chemical behaviors of

*Electronic address: halien@iop.vast.vn

[†]Electronic address: anh.phanduc@phenikaa-uni.edu.vn

nanostructures under laser irradiation. We use transmission electron microscopy (TEM) and X-ray diffraction (XRD) spectrum to analyze structures of experimental samples. Effects of DOX loading on optical properties are determined using the absorption spectrum. Then, we inject solutions of GNRs@mSiO₂ with and without DOX molecules into 45 normal and tumor-planted mice and study chemo-photothermal activities. Based on experimental results, we quantitatively evaluate roles of individual mechanism on cancer treatments.

II. EXPERIMENTAL SECTION

A. Materials

We purchased tetrachloroauric acid trihydrate 99.5 % (HAuCl₄ · 3H₂O), ethanol, CTAB, ascorbic acid, and AgNO₃ from Merck. Tetraethoxysilane and NH₄OH (28-30 %), and NaBH₄ were purchased from Sigma-Aldrich and Walko, respectively. Doxorubicin hydrochloride 2 mg/ml was provided by Ebewe Pharma. In our experiments, we dispersed materials into double distilled water.

B. Preparation and characterization of GNR@SiO₂-DOX complex

The synthesis of GNR@SiO₂-DOX composites consists of three steps. First, we synthesized near-infrared light-responsive GNRs. Second, a mesoporous silica layer is coated on gold surfaces. A thickness of the silica layer is approximately 15 nm. Third, when dispersing DOX.HCl molecules in an aqueous solution of GNRs, the mesoporous silica surface adsorbed the biomolecules onto the mesoporous silica surface via electrostatic interactions. Finally, we obtained mesoporous silica-encapsulated GNRs (GNR@mSiO₂-DOX) composites loading DOX molecules.

1. Preparation of GNRs

Gold nanorods having dimensions of $\sim 39.2 \times 10.7$ nm (an average aspect ratio of 3.7) were synthesized using the seed-mediated growth method [29]. Briefly, the seed was made by stirring 120 μ l of 25 mM HAuCl₄ in 10 ml of 100 mM CTAB solution. Then, we quickly added ice-cold NaBH₄ (60 μ l, 10 mM) to the seed solution and stirred for 2-6 hours. By mixing 100 ml of CTAB 100 mM, 1.5 ml of HAuCl₄ 25 mM, 450 μ l of AgNO₃ 25 mM and 270 μ l of L-ascorbic acid 100 mM, a growth solution was prepared. After 2 hours of reaction in a mixture of 1000 μ l of the seed solution and the growth solution, the GNR seeds were synthesized.

2. Preparation of mesoporous silica-encapsulated GNRs

GNRs were prepared by a seed-mediated sequential growth and a reduction of gold salt in the presence of in the presence of a CTAB surfactant. A 20 ml aliquot of the GNRs solution was centrifuged and re-dispersed in 20 ml deionized water. Then, we added 0.5 ml of the TEOS ethanol solution (20 mM) to 20 mL of GNR aqueous solution (pH is adjusted to 10-11 by mixing NH₄OH). After vigorously stirring for 24 hours at room temperature, there was a 15nm thick mesoporous silica layer forming on the surface of the GNRs through hydrolysis and condensation of TEOS. The silica-encapsulated GNRs were isolated by centrifugation, washed with deionized water and ethanol several times, and then re-dispersed in 2 ml of deionized water for later use.

3. Mesoporous silica-encapsulated GNRs functionalized with doxorubicin drugs

We added 200 μ l of DOX.HCl 2-mg/mL solution to a solution of GNRs@mSiO₂ solution which has the optical density (OD) equal to 12. Then, this mixture was stirred and mixed during 75h at room temperature in the dark. Electrostatic interaction between doxorubicin molecules and the mesoporous silica surface leads to molecular adsorption at particle surfaces [30, 31]. Finally, we used UV-VIS-NIR spectrometer to monitor the adsorbing procedure of DOX into mesoporous silica surface.

4. Measurements

In the final GNR suspension, GNRs@mSiO₂ and GNRs@SiO₂DOX were characterized by an ultraviolet/visible wavelength (UV-VIS-NIR) spectrophotometer (Shimadzu 2600) and dynamic light scattering. We examined sizes and shapes of GNRs by high resolution transmission electron microscopy (HRTEM, JEM2100-JEOL). Samples were prepared by placing one drop of the GNR suspension on a 200-mesh, copper grid with carbon (SPI Supplies, West Chester, Pennsylvania), and drying in a vacuum oven overnight. We used X-Ray diffraction to determine the chemical composition and crystalline of the obtained GNRs.

C. In-vivo experiments

For in vivo experiments, we used healthy male Swiss Albino mice (810 weeks old) with weight of 18 ± 1.5 g. The mice had free access to food and water and were maintained on a 14/10 h light/dark cycle. The sarcoma cancer cells were subcutaneously implanted (2×10^6 cells/100 μ l of Hanks solution) into the right side of mouse back. The tumor size was daily measured. These animals were examined when their average tumor size

grew up to 5-6 mm diameter. We randomly divided forty five mice into nine groups (five mice per groups): one control group and eight experimental groups with two different concentrations of GNR@mSiO₂ and GNR@mSiO₂-DOX having optical density of 5.5 and 9.2 at 808 nm under 808-nm laser irradiation. Particularly, the groups are

- Control group: without tumor and no treatment.
- Group 1: saline injection.
- Group 2: saline injection + 808-nm laser irradiation;
- Group 3: GNR@mSiO₂ OD = 9.2.
- Group 4: GNR@mSiO₂-DOX OD = 9.2
- Group 5: GNR@mSiO₂ OD = 5.5 + 808-nm laser irradiation.
- Group 6: GNR@mSiO₂ OD = 9.2 + 808-nm laser irradiation.
- Group 7: GNR@mSiO₂-DOX OD = 5.5 + 808-nm laser irradiation.
- Group 8: GNR@mSiO₂-DOX OD = 9.2 + 808-nm laser irradiation.

We used a 1 ml syring 26G needle to inject directly 30 μ l of phosphate-buffered saline (PBS) 1x or GNR@mSiO₂/GNR@mSiO₂-DOX solutions into each tumor center of mice. The animals were irradiated with laser (808 nm, 3.25 W/cm², 1 minute, a spot size of 6 mm) immediately after tumor-direct injection. The laser was focused on the center of the tumor. We measured the temperature rise of tumor surface by an infrared (IR) camera (Chauvin Arnoux C.A 1995 IR camera IP 54). After treatment, we observed health and weight of mice. After 1 month, all mice were euthanized. We dissected their tumors and measured their weight. Average body weights of nine groups of mice as a function of time were shown in Figure S1 in Supporting Information. At that time, we also analyzed blood chemistry and hematology. All experiments were performed in compliance with the policy on animal use and ethics.

III. RESULTS AND DISCUSSIONS

Figure 1a and 1b show TEM images of a solution of GNRs and GNR@mSiO₂, respectively. The TEM images indicate that the average length and width are 39.2 ± 6.2 nm and 10.7 ± 1.7 nm, respectively, (the average aspect ratio of 3.7). The silica shell is uniform and has thickness of ~ 15 nm. One can see a TEM image of the mesoporous silica coating on GNRs in Figure S2 in Supporting Information.

Figure 1c shows X-ray diffraction of GNRs to determine their chemical composition and crystalline. We find three characteristic diffraction peaks at 38.27° , 44.42° , and 64.70° corresponding to the (111), (200), and (220) crystal planes of the face-centered cubic structure of gold (JCPDS no. 04-0784), respectively. The presence of these optical maxima indicates a polycrystalline structure of GNRs. In addition, since there is no other impurities in the diffraction patterns, our samples are composed

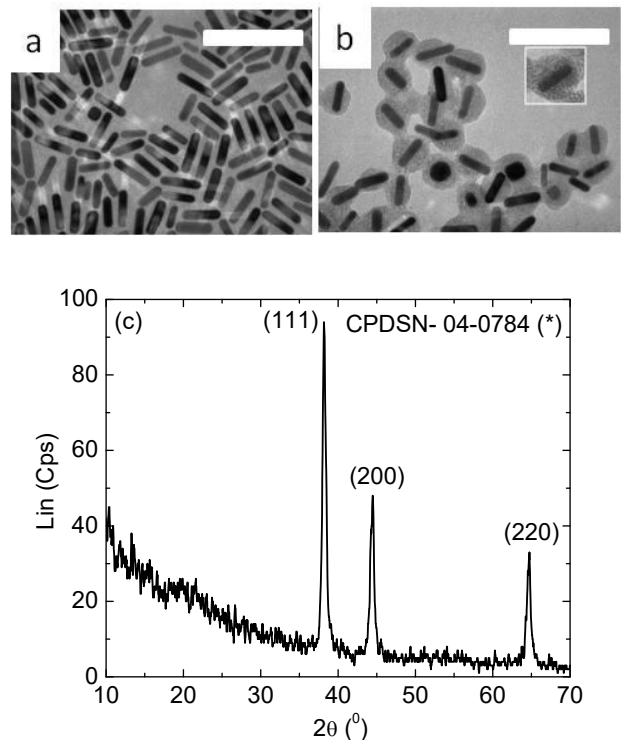


FIG. 1: (Color online) TEM image of (a) GNRs and (b) GNR@mSiO₂ with scale bar of 100 nm, and (c) X-ray diffraction spectrum of GNRs.

of pure crystalline gold.

Figure 2 shows normalized absorption spectra of GNRs (or CTAB-GNRs) and GNR@mSiO₂. Note that GNRs have CTAB molecules on the surface to stabilize and avoid aggregation. In each spectrum, two peaks corresponds to the transverse (~ 513 nm) and longitudinal (~ 820 nm) oscillation. The surface plasmon resonance of GNRs is strongly dependent on their aspect ratio [20]. An increase of the aspect ratio leads to a red-shift of the optical peak. However, our results indicates the silica layer has a minor effect on the absorption spectrum. This may be due to a broad distribution of the rod length and width of GNRs as shown in Figure S3 in Supporting Information. This behavior is completely consistent with experimental results in Ref. [32].

Compared to the optical spectrum of CTAB-GNRs, the longitudinal surface plasmon resonance band of GNR@mSiO₂ is slightly red-shifted about 6 nm. Meanwhile, the peak location for the transverse plasmon band of CTAB-GNRs is at 513 nm and this resonance is blue-shifted about 4 nm when coating silica on the gold surface. This behavior can be explained that the refractive index of silica shell (1.45) is closer to that of water media (1.33) than that of 2-3 nm CTAB layer (1.49). It means the silica layer provides more transmission and lower reflection of electromagnetic fields than the CTAB layer. Thus, more electrons of the GNR core are excited to collectively resonate. The shift of optical resonances as in-

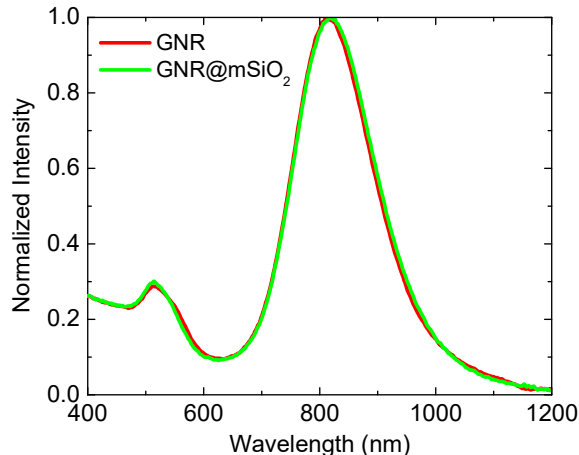


FIG. 2: (Color online) Normalized absorption spectra of GNRs and GNR@mSiO₂.

creasing the refractive index of the medium surrounding the core is predictable.

The DOX loading of GNRs@mSiO₂ can be analyzed using the absorption spectra. As shown in Figure 3, the absorption spectra of GNR@mSiO₂ is blue-shifted after adsorbing DOX. Doxorubicin molecules in the mesoporous silica layer enhance the absorbance intensity of the transverse peak near 500 nm but do not affect the absorbance of the longitudinal peak located at about 813 nm. This is because DOX molecules strongly absorb light at 500 nm and do not interact with NIR radiation. After 75 hours incubation, the optical spectrum of GNR@mSiO₂-DOX is lowered in comparison with the spectrum measured immediately before and after mixing DOX. These results indicate that DOX molecules tightly bind to the silica layer of GNR@mSiO₂ but biological degradation may appear [33].

Free and adsorbed DOX molecules can be separated using centrifugation. We removed the supernatant with a pipet and determined the concentration of the residual DOX in the supernatant by measuring its absorbance and then comparing this measured spectrum with that of known concentrations of free DOX solution. From this, we estimated that 1 μ g of Au approximately absorbs 1.3 μ g of DOX.

Under NIR 808-nm laser irradiation with power density at 3.25 W/cm² for 1 minute, GNRs@mSiO₂ and GNRs@mSiO₂-DOX in solutions absorb the light energy and convert it into heat. Solutions of plasmonic nanocomposites are fixed at the same optical density of 3.6 at 808 nm. During the laser illumination, as shown in Figure 4, temperature of GNR@mSiO₂ and GNR@mSiO₂DOX solutions rapidly increases from room temperature to approximately 70.5 °C. Theoretically, by using the energy balance equation in homogeneous and open systems, one derives an analytical fitting function $T(t) = T_0 + \frac{A}{B}(1 - e^{-Bt})$ to describe the time-

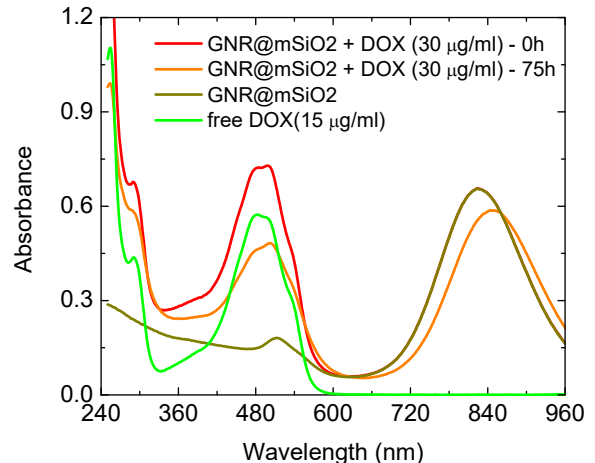


FIG. 3: (Color online) Absorption spectra of free DOX at concentration 30 μ g/ml, GNR@mSiO₂, GNR@mSiO₂-DOX (30 μ g/ml) at 0 hour and after 75 hours of incubation.

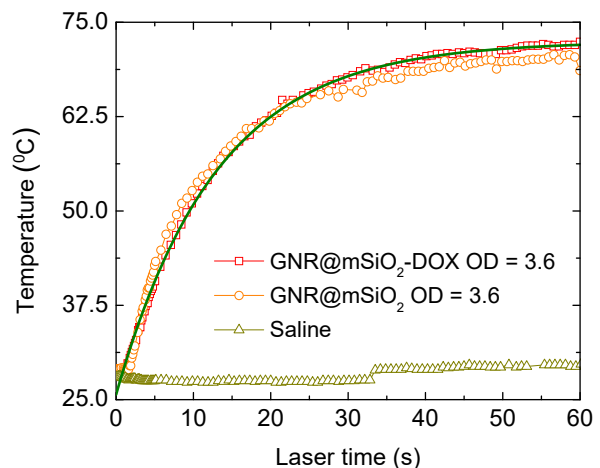


FIG. 4: (Color online) Time-dependent temperature of GNR@mSiO₂, GNR@mSiO₂-DOX solutions with optical density of 3.6 and saline irradiated with the NIR laser (808 nm, 3.25W/cm²). The solid curve is an analytic function $T(t) = T_0 + \frac{A}{B}(1 - e^{-Bt})$ with $T_0 = 24.67$ °C, $A \approx 3.168$ °C s, and $B = 0.0773$ s⁻¹.

dependent temperature [15, 34]. The analysis agrees quantitatively well with our experimental data. The temperature rises of these solutions relatively overlap. This result can be deduced from Figure 3 since the presence of DOX molecules does not alter the absorbance of GNR@mSiO₂ in the NIR region. Thus, aqueous solutions of GNR@mSiO₂ and GNR@mSiO₂DOX absorb energy and are heated in the same manner. While the temperature is nearly unchanged in saline solution.

Furthermore, since the absorption spectrum of GNRs with and without a mesoporous silica layer on the gold

surface have a very small variation (see Figure 2), one could expect a perfect overlapping between the time-dependent temperature rise of GNR solution and that of GNR@mSiO₂ solution.

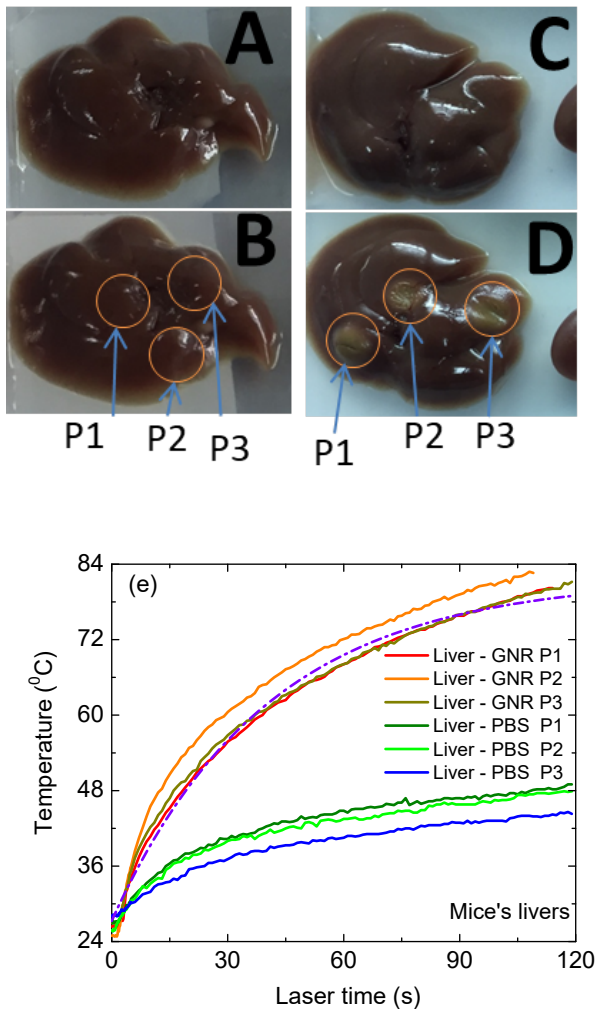


FIG. 5: (Color online) The liver of control mouse image without GNR infusion image before (a) and after (b) irradiated by NIR laser irradiation (808 nm, 3.5 W/cm², 2 minutes). The liver of mouse image with 150 μ l, OD = 10 of GNR@mSiO₂ infusion before (c) and after (c) NIR laser radiation (808 nm, 3.25 W/cm², 2 minutes). (e) Temperature rises of mice liver at the three different positions after vein tail injection 2 hours in (b) and (d). The dashed-dotted violet curve is the analytic function $T(t) = T_0 + \frac{A}{B}(1 - e^{-Bt})$ with $T_0 = 27.29$ °C, $A \approx 1.36$ °C s, and $B = 0.025$ s⁻¹.

Examining chemo-photothermal effects of nanocomposites on animals is an essential part to step towards practical applications. In addition to investigations of the time-dependent temperature rise, the liver accumulation of nanostructures has been intensively concerned in medical-related fields. Several recent works used the dose for intravenous administration of GNRs ranging from 1.7

mg · kg⁻¹ to 25 mg · kg⁻¹ [9, 35]. It was proved that the amount of GNRs is accumulated in internal organs, particularly in liver and spleen after infusion. In the remaining life, GNRs cannot be excreted from their bodies [27]. Another study showed that gold nanoparticles are mainly trapped in the Kuffer macrophage cells in the liver for 2 hours after intravenous injection [36].

In our work, to test the accumulation of GNR@mSiO₂ in the liver, we used low doses (100 μ l of saline buffer and GNR@mSiO₂ 1.75 mg · kg⁻¹) to inject into mice. For two hours after intravenous injection, mice were sacrificed and their livers were taken. The presence and influences of GNRs in the livers were determined via photothermal effects. Under the same conditions of *in vivo* experiments, we illuminated livers at the three different positions (P_1 , P_2 , and P_3 as depicted in Figure 5b and 5d) within 2 min of NIR laser (808 nm, 3.25 W/cm²). For livers without GNRs, Figure 5a and 5b show no difference (visual) between before and after laser radiation at three irradiated positions. Meanwhile, for livers of mice with tail vein injection of GNR@mSiO₂ solutions, one visually observes color change of the liver after laser radiation in Figure 5d. Color at these three positions irradiated by laser turns yellow compared to Figure 5c. This indicates the presence of gold nanostructures in the liver and the accumulation leads to the heat-induced denaturation of organs. The time-dependent temperature rises of livers at positions P_1 , P_2 , and P_3 in Figure 5b and d, which correspond samples injected by saline buffer and GNR@mSiO₂, respectively, were monitored and shown in Figure 5e. The temperatures of experimental samples with GNRs@mSiO₂ increase up to 85 ± 2 °C after 2 minutes. For liver with only saline, the temperature slowly increases and reaches to 44 ± 1 °C. There is no much difference between temperatures at the irradiated points. This finding suggests that the liver is an approximately homogeneous medium and GNRs@mSiO₂ are randomly distributed. Again, the mathematical form of the time-dependent temperature obeys the fit equation $T(t) = T_0 + \frac{A}{B}(1 - e^{-Bt})$.

The chemo- and photothermal therapies in mice due to the use of GNR@SiO₂ and GNR@SiO₂-DOX are also investigated by the implanted mouse tumor models as described in Section II. C. Figure 6a shows photographs of tumors taken from 8 animal groups after 30 days treatment. We measured the average tumor weight of each group. The results are shown in Figure 6b to quantify contribution of chemotherapy and photothermal therapy. Overall, the presence of GNR@SiO₂ and GNR@SiO₂-DOX without laser exposure destroys tumor cells. Treatment efficiency of using laser illumination on tumors without plasmonic nanostructures is better than just only using GNRs@SiO₂ without laser illumination. However, coating DOX molecules onto the plasmonic composites (group 4) approximately reduces the tumor volume and weight by a factor of 1.5 and 2.7 compared to only GNR@SiO₂ (group 3) and saline injection (group 1), respectively. By turning on the NIR laser light

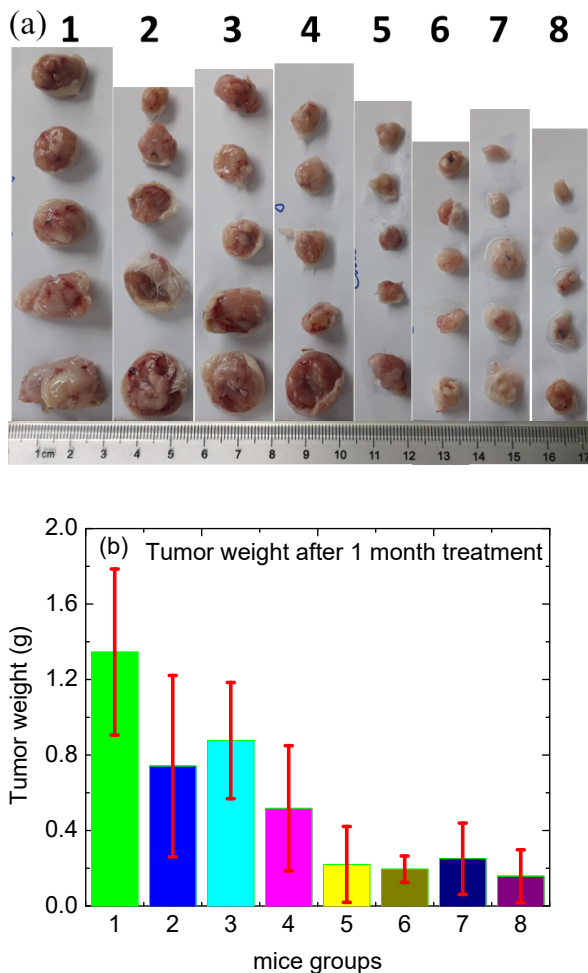


FIG. 6: (Color online) (a) Photograph of tumors after excision from 8 groups. (1) untreated group, (2) laser only, (3) treatment with GNR@SiO₂ OD = 9.2, (4) treatment with GNR@SiO₂-DOX OD = 9.2. (5) and (6) treatment with GNR@SiO₂ OD = 5.5 and 9.2, respectively, (7) and (8) treatment with GNR@SiO₂-DOX OD = 5.5 and 9.2, respectively, and under NIR laser irradiation (808 nm, 3.25 W/cm², 1 minute). (b) The average tumor weights of each group.

when tumors have GNR@SiO₂-DOX, we combine effects of the anti-cancer drug and photothermal agents. This combination significantly enhances the efficiency and effectiveness of GNR@SiO₂-DOX dose. Using more photothermal agents enables to absorb more optical energy to thermally devastate tumor tissue. One can deduce this conclusion from comparing group 7 and 8, which correspond injections with the optical density of 5.5 and 9.2, respectively.

IV. CONCLUSIONS

We have validated anti-cancer effects of the chemophotothermal therapy based on GNR@SiO₂-DOX by *in vivo* experiments. We have experimentally prepared

GNR@SiO₂-DOX and examined complex structures via SEM and TEM image, and XRD technique. Based on absorption spectra, one can observe variations of plasmonic properties of GNRs of size 10.7 nm × 39.2 nm when coating a mesoporous silica layer on the gold surface and encapsulating DOX molecules onto this silica layer. Moreover, these optical spectra allow us to determine the amount of loaded DOX molecules. After injecting solutions of the GNR@SiO₂ and GNR@SiO₂-DOX into mice and scarifying them, photothermal experiments are carried out in both water and livers of mice. These experiments proves that GNRs@SiO₂ are accumulated in livers. The mice liver can be approximately considered as a homogeneous medium and the injected GNRs are randomly dispersed in the liver when injected into mice. When we inject solutions of GNRs@SiO₂ and GNRs@SiO₂-DOX into tumor-implanted mice and irradiate NIR laser light on their tumors within 1 minute immediately after direct injection, health and weight of mice are observed everyday for one month. Then, their tumors are taken to measure weight. All measurements explicitly indicate that both chemotherapy and photothermal therapy significantly reduce tumor volumes. More reduction of volumes is found when combining these two approaches.

Conflicts of interest

There are no conflicts to declare.

Acknowledgments

The animal experiment and all *in vivo* studies were performed according to ethical approval (IRB-A-2001) and guidelines of Institutional Review Board in Animal Research at Dinh Tien Hoang Institute of Medicine, Hanoi, Vietnam. The authors are grateful for the financial support for this work from the project VAST.CTVL.02/17-18 and the project 103.03-2016.72 of the Vietnam National Foundation for Science and Technology Development (NAFOSTED).

Author Information

Corresponding authors: anh.phanduc@phenikaa-uni.edu.vn, halien@iop.vast.vn

Supporting Information

Average body weight of nine groups of mice *in vivo* in experiments as a function of time, TEM image of the mesoporous silica coating on GNRs, and histogram of the rod length and width of GNRs.

- [1] Huang, X.; Jain, P. K.; El-Sayed, I. H.; El-Sayed, M. A. Plasmonic photothermal therapy (PPTT) using gold nanoparticles. *Lasers Med. Sci.* **2008**, *23*, 217-228.
- [2] Abadeer, N. S.; Murphy, C. J. Recent Progress in Cancer Thermal Therapy Using Gold Nanoparticles. *J. Phys. Chem. C* **2016**, *120*, 46914716.
- [3] Cole, J. R.; Mirin, N. A.; Knight, M. W.; Goodrich, G. P.; Halas, N. J. Photothermal Efficiencies of Nanoshells and Nanorods for Clinical Therapeutic Applications. *J. Phys. Chem. C* **2009**, *113*, 12090-12094.
- [4] Link, S.; El-Sayed, M. A. Shape and size dependence of radiative, non-radiative and photothermal properties of gold nanocrystals. *Int. Rev. Phys. Chem.* **2000**, *19*, 409-453.
- [5] Link, S.; Burda, C.; Mohamed, M. B.; Nikoobakht, B.; El-Sayed, M. A. Laser Photothermal Melting and Fragmentation of Gold Nanorods: Energy and Laser Pulse-Width Dependence. *J. Phys. Chem. A* **1999**, *103*, 11651170.
- [6] O'Neal, D. P.; Hirsch, L. R.; Halas, N. J.; Payne, J. D.; West, J. L. Photo-thermal tumor ablation in mice using near infrared-absorbing nanoparticles. *Cancer Lett.* **2004**, *209*, 171-176.
- [7] Wang, L.; Jiang, X.; Ji, Y.; Ru Bai, Zhao, Y.; Wu, X.; Chen, C. Surface chemistry of gold nanorods: origin of cell membrane damage and cytotoxicity. *Nanoscale* **2013**, *5*, 8384-8391.
- [8] Yasun, E.; Li, C.; Barut, I.; Janvier, D.; Qiu, L.; Cui, C.; Tan, W. BSA modification to reduce CTAB induced non-specificity and cytotoxicity of aptamer-conjugated gold nanorods. *Nanoscale* **2015**, *7*, 1024010248.
- [9] Shen, S.; Tang, H.; Zhang, X.; Ren, J.; Pang, Z.; Wang, D.; Gao, H.; Qian, Y.; Jiang, X.; Yang, W. Targeting Mesoporous Silica-Encapsulated Gold Nanorods for Chemo-Photothermal Therapy with Near-Infrared Radiation. *Biomaterials* **2013**, *34*, 3150-3158.
- [10] Vallet-Regi, M.; Colilla, M.; Izquierdo-Barba, I.; Manzano, M. Mesoporous Silica Nanoparticles for Drug Delivery: Current Insights. *Molecules* **2017**, *23*, 47.
- [11] Yang, H.; Xu, M.; Li, S.; Shen, X.; Li, T.; Yan, J.; Zhang, C.; Wu, C.; Zeng, H.; Liu, Y. Chitosan hybrid nanoparticles as a theranostic platform for targeted doxorubicin/VEGF shRNA co-delivery and dual-modality fluorescence imaging. *RSC Adv.* **2016**, *6*, 29685-29696.
- [12] Chai, F.; Sun, L.; He, X.; Li, J.; Liu, Y.; Xiong, F.; Ge, L.; Webster, T.J.; Zheng, C. Doxorubicin-loaded poly (lactic-co-glycolic acid) nanoparticles coated with chitosan/alginate by layer by layer technology for antitumor applications. *Int. J. Nanomed.* **2017**, *12*, 1791.
- [13] Li, G.; Chen, Y.; Zhang, L.; Zhang, M.; Li, S.; Li, L.; Wang, T.; Wang, C. Facile Approach to Synthesize Gold Nanorod@Polyacrylic Acid/Calcium Phosphate YolkShell Nanoparticles for Dual-Mode Imaging and pH/NIR-Responsive Drug Delivery. *Nano-Micro Lett.* **2017**, *10*, 7.
- [14] Zhang, Z.; Wang, J.; Nie, X.; Wen, T.; Ji, Y.; Wu, X.; Zhao, Y.; Chen, C. Near infrared laser-induced targeted cancer therapy using thermoresponsive polymer encapsulated gold nanorods. *J. Am. Chem. Soc.* **2014**, *136*, 7317-7326.
- [15] Duong, V. T. T.; Phan, A. D.; Lien, N. T. H.; Hue, D. T.; Hoa, D. Q.; Nga, D. T.; Nhung, T. H.; Viet, N. A. Near-Infrared Photothermal Response of Plasmonic Gold-Coated Nanoparticles in Tissues. *Phys. Status Solidi A* **2018**, *215*, 1700564.
- [16] Ayala-Orozco, C.; Urban, C.; Knight, M. W.; Urban, A. S.; Neumann, O.; Bishnoi, S. W.; Mukherjee, S.; Goodman, A. M.; Charron, H.; Mitchell, T.; Shea, M.; Roy, R.; Nanda, S.; Schiff, R.; Halas, N. J.; Joshi, A. Au Nanomatryoshkas as Efficient Near-Infrared Photothermal Transducers for Cancer Treatment: Benchmarking against Nanoshells. *ACS Nano* **2014**, *8*, 6372-6381.
- [17] Wiley, D. T.; Webster, P.; Gale, A.; Davis, M. E. Transcytosis and brain uptake of transferrin-containing nanoparticles by tuning avidity to transferrin receptor. *Proc. Natl. Acad. Sci. U.S.A.* **2013**, *110*, 8662-8667.
- [18] Blanco, E.; Shen, H.; Ferrari, M. Principles of nanoparticle design for overcoming biological barriers to drug delivery. *Nat. Biotechnol.* **2015**, *33*, 941-951.
- [19] Kessentini, S.; Barchiesi, D. Quantitative Comparison of Optimized Nanorods, Nanoshells and Hollow Nanospheres for Photothermal Therapy Biomed. *Opt. Express.* **2012**, *3*, 590-604.
- [20] Kim, M.; Lee, J.-H.; Nam, J.-M. Plasmonic Photothermal Nanoparticles for Biomedical Applications. *Adv. Sci.* **2019**, *6*, 1900471.
- [21] Pigram, W. J.; Fuller, W.; Hamilton, L. D. Stereochemistry of Intercalation: Interaction of Daunomycin with DNA. *Nature New Biol.* **1972**, *235*, 1719.
- [22] Tacar, O.; Sriamornsak, P.; Dass, C. R. Doxorubicin: an update on anticancer molecular action, toxicity and novel drug delivery systems: Doxorubicin cell and molecular biological activity. *J. Pharm. Pharmacol.* **2013**, *65*, 157170.
- [23] Waterhouse, D. N.; Tardi, P. G.; Mayer, L. D.; Bally, M. B. A Comparison of Liposomal Formulations of Doxorubicin with Drug Administered in Free Form: Changing Toxicity Profiles. *Drug Saf.* **2001**, *24*, 903920.
- [24] Zhang, M.; Jiang, L. Doxorubicin Hydrochloride-Loaded Mesoporous Silica Nanoparticles Inhibit Non-Small Cell Lung Cancer Metastasis by Suppressing VEGF-Mediated Angiogenesis. *J. Biomed. Nanotechnol.* **2016**, *12*, 19751986.
- [25] Liu, Y.; Xu, M.; Chen, Q.; Guan, G.; Hu, W.; Zhao, X.; Qiao, M.; Hu, H.; Liang, Y.; Zhu, H.; Chen, D. Gold nanorods/mesoporous silica-based nanocomposite as theranostic agents for targeting near-infrared imaging and photothermal therapy induced with laser. *Int. J. Nanomed.* **2015**, *10*, 4747-4761.
- [26] Schwartz, J. A.; Shetty, A. M.; Price, R. E.; Stafford, R. J.; Wang, J. C.; Uthamantil, R. K.; Pham, K.; McNichols, R. J.; Coleman, C. L.; Payne, J. D. Feasibility study of particle-assisted laser ablation of brain tumors in orthotopic canine model. *Cancer Res.* **2009**, *69*, 1659-1667.
- [27] Gad, S. C.; Sharp, K. L.; Montgomery, C.; Payne, J. D.; Goodrich, G. P. Evaluation of the Toxicity of Intravenous Delivery of Auroshell Particles (GoldSilica Nanoshells). *Int. J. Toxicol.* **2012**, *31*, 584-594.
- [28] Rastinehad, A. R.; Anastos, H.; Wajswol, E.; Winoker, J. S.; Sfakianos, J. P.; Doppalapudi, S. K.; et al. Gold nanoshell-localized photothermal ablation of prostate tu-

- mors in a clinical pilot device study. *Proc. Natl. Acad. Sci. U.S.A.* **2019**, *116*, 18590-18596.
- [29] Ye, X.; Jin, L.; Caglayan, H.; Chen, J.; Xing, G.; Zheng, C.; Doan-Nguyen, V.; Kang, Y.; Engheta, N.; Kagan, C. R.; et al. Improved Size-Tunable Synthesis of Monodisperse Gold Nanorods through the Use of Aromatic Additives. *ACS Nano* **2012**, *6*, 2804-2817.
- [30] Shen, J.; He, Q.; Gao, Y.; Shi, J.; Li, Y. Mesoporous silica nanoparticles loading doxorubicin reverse multidrug resistance: performance and mechanism. *Nanoscale* **2011**, *3*, 4314-4322.
- [31] Yan, T.; Cheng, J.; Liu, Z.; Cheng, F.; Wei, X.; He, J. pH-Sensitive mesoporous silica nanoparticles for chemophotodynamic combination therapy. *Coll. Surf. B Biointerfaces* **2018**, *161*, 442-448.
- [32] Li, C.; Feng, K.; Xie, N.; Zhao, W.; Ye, L.; Chen, B.; Tung, C.-H.; Wu, L.-Z. Mesoporous Silica-Coated Gold Nanorods with Designable Anchor Peptides for Chemophotothermal Cancer Therapy. *ACS Appl. Nano Mater.* **2020**, DOI: 10.1021/acsnm.0c00311.
- [33] Beijnen, J. H.; Wiese, G.; Underberg, W. J. Aspects of the chemical stability of doxorubicin and seven other anthracyclines in acidic solution. *Pharm. Weekbl. Sci.* **1985**, *21*, 109-116.
- [34] Richardson, H. H.; Carlson, M. T.; Tandler, P. J.; Hernandez, P.; Govorov, A. O. Experimental and Theoretical Studies of Light-to-Heat Conversion and Collective Heating Effects in Metal Nanoparticle Solutions. *Nano Lett.* **2009**, *9*, 1139-1146.
- [35] von Maltzahn, G.; Park, J. H.; Agrawal, A.; Bandaru, N. K.; Das, S. K.; Sailor, M. J.; Bhatia, S. N. Computationally Guided Photothermal Tumor Therapy Using Long-Circulating Gold Nanorod Antennas. *Cancer Res.* **2009**, *69*, 3892-3900.
- [36] Sadauskas, E.; Wallin, H.; Stoltenberg, M.; Vogel, U.; Doering, P.; Larsen, A.; Danscher, G. Kupffer Cells Are Central in the Removal of Nanoparticles from the Organism. *Part. Fibre Toxicol.* **2007**, *4*, 10.